

BB plot: A Tool for Accurate Model Selection Using Bayes factors

Ankur Barsode*

International Centre for Theoretical Sciences, Tata Institute of Fundamental Research, Bangalore 560089, India

A common task in physics and astronomy is studying which of the competing hypotheses the data prefer. This is usually done by computing the Bayes factor between the two hypotheses, and either interpreting it in terms of the posterior odds or as a ranking statistic for a frequentist p-value test. Here we describe a relationship between the Bayes factor and its distributions under the two competing hypotheses, called the Bayes factor-Bayes factor (*BB*) relationship, expressed as a diagnostic plot. Using examples from gravitational wave (GW) astronomy, we demonstrate how the *BB* plot can validate the accuracy of Bayes factor calculations. The *BB* relationship may also be useful for estimating background distributions of the Bayes factor at low computational cost, even analytically in some cases. We apply this technique in the context of wave-optics lensing of GWs, extrapolating the background distribution from GWTC4 to put a rough bound of $\lesssim 4.1\sigma$ on the statistical significance of GW231123.

Keywords: Bayesian statistics, model selection

I. INTRODUCTION

Model selection is a central task in many areas of physics and astronomy, where one seeks to determine which among the proposed hypotheses are consistent with the observations, and which must be rejected. It lies at the heart of most major scientific discoveries that confirmed or challenged prevailing scientific theories [1–6]. In modern applications, this task is typically statistical in nature and often involves comparing the relative plausibility of models given noisy observations.

In the Bayesian approach, we compute the posterior odds in favor of one hypothesis over another. This is encoded by the Bayes factor, which is the ratio of evidences of data under each hypothesis, to be compared against an empirical scale (for eg, Jeffrey’s [7]) for interpretation.

On the other hand, the frequentist approach seeks to reject a “null” hypothesis based on a test “statistic” whose value is compared with its “background” distribution under the null hypothesis. The statistical significance is then expressed using the false positive probability (FPP), often quoted in terms of Gaussian significance; with $\geq 5\sigma$ usually considered a decisive detection. It is imperative that the statistic be appropriately chosen to maximize the efficiency of detecting the phenomenon of interest, while simultaneously minimizing false alarms. Such a statistic happens to be the Bayes factor itself [8].

Thus, accurate Bayes factors provide the basis for detection under both of these approaches. However, they may be challenging to calculate exactly due to the complexity of realistic models and limited computational resources. Approximations are often made, which raises a question of how correct they really are. Also, as human researchers, we must acknowledge the possibility that our calculations could have errors.

If the (numerically) exact calculation of the Bayes factor using, for eg, nested sampling [9, 10], is possible, only

computationally expensive, we may consider validating our approximation of the Bayes factor in a few, typical examples by comparing it against the exact answer. However, if such ground truth is too expensive to obtain, we must resort to internal consistency checks, such as those based on theorems by Alan Turing (the Good checks [11–13]) or other simulation based checks [14, 15].

In this paper, we present a discussion of a simulation based validation approach introduced in [16]. This approach, called the Bayes factor-Bayes factor or *BB* plot, can (i) provide a direct and internally consistent diagnostic for assessing the accuracy of approximate Bayes factor calculations without requiring access to ground-truth results, (ii) guide the systematic improvement of such approximations, and (iii) help construct computationally efficient estimates of frequentist background distributions, including semi-analytical extrapolations to regimes inaccessible to brute-force simulations. We illustrate these ideas using applications in gravitational wave (GW) astronomy, including waveform distortion searches and strong lensing, and apply them to place bounds on the statistical significance of GW231123 [17].

This paper is structured as follows: in Sec. II we provide a primer on Bayesian analysis and the *BB* plot. In Sec. III, we demonstrate benchmarking using *BB* plot in two model selection problems in GW astronomy. In Sec. IV, we estimate backgrounds for gravitational lensing of GWs using the *BB* relationship and estimate an upper bound on the statistical significance of GW231123. Our conclusions are presented in Sec. V.

II. THE BAYES FACTOR-BAYES FACTOR (*BB*) PLOT

At the heart of Bayesian model selection lies the Bayes theorem

$$P(\vec{\theta}_i | d, \mathcal{H}_i) = \frac{P(d | \vec{\theta}_i, \mathcal{H}_i) P(\vec{\theta}_i | \mathcal{H}_i)}{P(d | \mathcal{H}_i)} \quad (1)$$

* ankur.barsode@icts.res.in

which, for a model hypothesis \mathcal{H}_i , expresses the posterior distribution of model parameters $\vec{\theta}_i$, given data d , in terms of the likelihood of getting the data given those parameters $P(d | \vec{\theta}_i, \mathcal{H}_i)$, and their prior distribution $P(\vec{\theta}_i | \mathcal{H}_i)$. The denominator on the right is the Bayesian evidence that normalizes the posterior

$$P(d | \mathcal{H}_i) = \int d\vec{\theta}_i P(d | \vec{\theta}_i, \mathcal{H}_i) P(\vec{\theta}_i | \mathcal{H}_i) \quad (2)$$

The Bayes factor is defined as the ratio of evidences under different model hypotheses, say, for $i = 1, 2$,

$$\mathcal{B}_2^1(d) = \frac{P(d | \mathcal{H}_1)}{P(d | \mathcal{H}_2)}. \quad (3)$$

It is often called the *likelihood ratio* of the competing models for producing the observed data. Note that the Bayes factor also implicitly depends on the prior choices under each hypothesis, apart from being an explicit function of the data.

It is useful to clarify what is meant by “data” in this context. The raw numbers recorded by the instruments typically pass through a pipeline of processes that reduce, refine, and simplify them. For a given observation, the data product at the end of every intermediate process in this pipeline should, in principle, give the same Bayes factor. Ultimately, we might consider the calculation of the Bayes factor itself as a process that returns “data” (= the Bayes factor) using which we could compute the Bayes factor. Thus

$$\mathcal{B}_2^1 = \frac{P(\mathcal{B}_2^1 | \mathcal{H}_1)}{P(\mathcal{B}_2^1 | \mathcal{H}_2)}, \quad (4)$$

where the Bayes factor is being treated as a random variable, and the equality holds at the level of its probability densities under each hypothesis.

More formally, we can derive the above relationship by noting that the probability density of the Bayes factor is given by marginalizing over all possible data that result in that Bayes factor. For the hypothesis \mathcal{H}_1 , this is

$$P(\mathcal{B}_2^1 | \mathcal{H}_1) = \int dd P(d | \mathcal{H}_1) \delta(\mathcal{B}_2^1 - b(d)) \quad (5)$$

where δ is the Dirac delta function, and we are temporarily denoting the Bayes factor function by $b(d)$ to avoid confusion with the Bayes factor as a random variable \mathcal{B}_2^1 . Using the definition in Eq. (3), we can substitute $P(d | \mathcal{H}_1)$ by $b(d) \cdot P(d | \mathcal{H}_2)$

$$P(\mathcal{B}_2^1 | \mathcal{H}_1) = \int dd b(d) P(d | \mathcal{H}_2) \delta(\mathcal{B}_2^1 - b(d)). \quad (6)$$

The Dirac delta function restricts the integral to those data realizations for which $b(d) = \mathcal{B}_2^1$. On this support, $b(d)$ can therefore be treated as a constant within the integral. This gives

$$P(\mathcal{B}_2^1 | \mathcal{H}_1) = \mathcal{B}_2^1 \int dd P(d | \mathcal{H}_2) \delta(\mathcal{B}_2^1 - b(d)). \quad (7)$$

The integral is analogous to Eq. (5), only in this case it gives the distribution of Bayes factors under the hypothesis \mathcal{H}_2 , resulting in

$$P(\mathcal{B}_2^1 | \mathcal{H}_1) = \mathcal{B}_2^1 P(\mathcal{B}_2^1 | \mathcal{H}_2), \quad (8)$$

which is identical to Eq. (4). Thus, the ratio of the PDFs of \mathcal{B}_2^1 under the competing hypotheses at various values of \mathcal{B}_2^1 should be equal to the corresponding \mathcal{B}_2^1 .

We will refer to this relationship between the Bayes factor and its distributions under the competing hypotheses as the Bayes factor-Bayes factor or *BB* relationship. Multiplying both sides of Eq. (8) by \mathcal{B}_2^{1n} and integrating over \mathcal{B}_2^1 , we recover the Turing-Good theorem that the expectation value of \mathcal{B}_2^{1n} under hypothesis \mathcal{H}_1 is equal to that of \mathcal{B}_2^{1n+1} under \mathcal{H}_2 . In particular, $n = 0$ gives the rather surprising result that the average value of the Bayes factor under the “null” (i.e., \mathcal{H}_2) hypothesis is 1. Previous work proposed to use these expectation values for diagnostics [12, 13], though there has been some criticism [15].

The *BB* relationship can directly be used as a diagnostic test by making a *BB* plot: a graph of the right-hand side of Eq. (4) against its left-hand side. It is expected to lie on the diagonal equality line. There may be fluctuations due to finite sampling noise, but these can be estimated using, for eg, bootstrapping methods.

Practically, we perform two separate experiments: first, we generate random realizations of data from the prior corresponding to the first hypothesis. For each such realization, we compute the Bayes factor, effectively obtaining a large number of samples from which the distribution $P(\mathcal{B}_2^1 | \mathcal{H}_1)$ can be empirically reconstructed using, for eg, histograms. In the second experiment, we repeat the same procedure but with data generated using the prior corresponding to the second hypothesis to empirically construct $P(\mathcal{B}_2^1 | \mathcal{H}_2)$. Since the data in each experiment is generated from its respective prior, and *both* the priors enter the calculation of Bayes factor, it should not be too surprising that the distributions $P(\mathcal{B}_2^1 | \mathcal{H}_1)$ and $P(\mathcal{B}_2^1 | \mathcal{H}_2)$, though obtained using data from two independent experiments, are nevertheless related to each other. Equation (4) is precisely that relationship, and is visualized by plotting the ratio of these empirical reconstructions against \mathcal{B}_2^1 .

Bayesian model selection involves interpreting the Bayes factor at face value, necessitating accuracy. On the other hand, frequentist model selection requires expensive simulations and data processing to generate the “background” $P(\mathcal{B}_2^1 | \mathcal{H}_2)$ and “foreground” $P(\mathcal{B}_2^1 | \mathcal{H}_1)$ distributions for estimating the False Positive (FPP) and False Dismissal (FDP) probabilities, respectively. The *BB* plot connects the quantities these two approaches rely upon, making it possible to use one for obtaining the other. In subsequent sections, we will show how the *BB* plot can be used to benchmark the accuracy of Bayes factors using simulated backgrounds and foregrounds. If a validated Bayesian methodology exists, we show how

the BB plot can help estimate its background at low computational cost.

III. BENCHMARKING BAYES FACTORS

The Bayes factor is analytically tractable in only a few, limited cases; realistic data and models are often too complicated to enable a direct evaluation of the evidences in Eq. (2). While recent developments in nested sampling and computing hardware have made it possible to evaluate evidences in several real-life problems, it still remains relatively expensive, and we often resort to making approximations to simplify the calculations at the risk of incurring some error.

The BB plot can help us quantify such errors. If it is possible to simulate data under each of the competing hypotheses, we could generate a large number of such data, evaluate our approximation $\hat{\mathcal{B}}_2^1$ of the Bayes factor on them, and empirically construct the distributions $P(\hat{\mathcal{B}}_2^1 | \mathcal{H}_1)$ and $P(\hat{\mathcal{B}}_2^1 | \mathcal{H}_2)$. If our approximation is correct, a BB plot of $P(\hat{\mathcal{B}}_2^1 | \mathcal{H}_1)/P(\hat{\mathcal{B}}_2^1 | \mathcal{H}_2)$ against $\hat{\mathcal{B}}_2^1$ will lie close to the equality line, while deviations may help identify potential discrepancies.

We caution, however, that satisfying the BB plot alone is not sufficient to deem the Bayes factor calculation as correct. A trivial counterexample is when we define $\hat{\mathcal{B}}_2^1 = P(S | \mathcal{H}_1)/P(S | \mathcal{H}_2)$, where S can be an arbitrary scalar function of the random realizations of data. Multiplying and dividing this equation by $dS/d\hat{\mathcal{B}}_2^1$, it is easy to recognize that this will satisfy Eq. (4), even though $\hat{\mathcal{B}}_2^1$ may be completely different from the true Bayes factor one would obtain from Eq. (3).

Nevertheless, while the efficiency may be degraded relative to that corresponding to the true Bayes factor, $\hat{\mathcal{B}}_2^1$ is still interpretable in the Bayesian sense of relative odds. Also, if we are systematically approximating the exact expression of the Bayes factor (rather than working with the likelihood ratio of an arbitrary statistic), it appears (though we provide no rigorous proof) that such a caveat may be unimportant.

A. Gravitational Waveform Distortion

One of the motivations behind GW astronomy is to test the theory of General Relativity (GR) in the extreme conditions around a compact binary merger. Any deviations would end up distorting the waveforms of the GWs from our expectations under GR (see, for eg, [18]). Such distortions could also be caused by gravitational lensing of GWs [19–21], and we will return to this in Sec. IV B. In this section, we will focus on a toy model that captures the main spirit of the search for generic waveform distortion effects, and show how the BB plot may assist in improving these searches.

Our problem consists of a fiducial “GR” signal

$$h_{\text{GR}}(t; A, \sigma) = A \sin(100t) e^{-t^2/2\sigma^2} \quad (9)$$

given by a Gaussian with amplitude A and width σ modulating a sine wave, and an alternative to GR “AG” signal

$$h_{\text{AG}}(t; A, \sigma, \tau) = \begin{cases} A \sin(100t) e^{-t^2/2\sigma^2}, & \text{if } t \leq 0 \\ A \sin(100t) e^{-t^2/2\sigma^2} e^{-t/\tau}, & \text{otherwise} \end{cases} \quad (10)$$

having an additional exponential decay with timescale τ beyond the peak amplitude, standing in for the waveform distortion. For $\tau \gg \sigma$, the distortion is small, and the AG and GR signals are almost identical.

The priors describing these signals’ parameters are assumed to be loguniform with ranges $A \in [0.01, 10]$, $\sigma \in [0.1, 10]$ for both GR and AG models, with $\tau \in [0.1, 10]$ in the AG model. Only those regions of the prior space that result in optimal signal-to-noise ratio (SNR) $\rho_{\text{opt}} \geq 8$ in standard normal white noise are considered, where ρ_{opt} is defined by

$$\rho_{\text{opt}} = \sqrt{\int_{-\infty}^{\infty} dt h_i^2(t; \vec{\theta}_i)} \quad (11)$$

where h_i and $\vec{\theta}_i$ stand for the waveform and parameters of a particular model, $h_1 = h_{\text{GR}}$ and $\vec{\theta}_1 = \{A, \sigma\}$ for GR, and $h_2 = h_{\text{AG}}$ and $\vec{\theta}_2 = \{A, \sigma, \tau\}$ for AG.

For either of these models, we can draw a random parameter point from the appropriate prior, generate a signal according to the waveform models in Eqs. (9) or (10), and inject (i.e., add) it in standard normal white noise to generate a mock data strain $d(t)$. Given $d(t)$, the functional forms of the two waveform models, and the two priors, we would like to identify whether the injected signal was AG or GR.

It is straightforward to set up the Bayesian model selection formalism. The log-likelihood is given by

$$\ln P(d | \vec{\theta}_i) = -\ln 2\pi - \frac{1}{2} \int_{-\infty}^{\infty} dt (d(t) - h_i(t; \vec{\theta}_i))^2. \quad (12)$$

with $i = 1$ for the AG model and 2 for the GR model, and we have dropped the explicit dependence on \mathcal{H}_i since $\vec{\theta}_i$ already fixes it. This, combined with the priors defined above, can be fed into a nested sampler such as, for eg, NAUTILUS [22], to sample the posterior distributions (Eq. (1)) and calculate the evidences (Eq. (2)) under each of the two hypotheses, which would then give the Bayes factor

$$\mathcal{B}_2^1 = \frac{\int d\vec{\theta}_1 P(d | \vec{\theta}_1) P(\vec{\theta}_1 | \mathcal{H}_1)}{\int d\vec{\theta}_2 P(d | \vec{\theta}_2) P(\vec{\theta}_2 | \mathcal{H}_2)}. \quad (13)$$

However, while the problem posed above is simple enough, most realistic gravitational waveform distortion effects require sampling 15 or higher dimensional likelihoods, involving millions of likelihood evaluations that

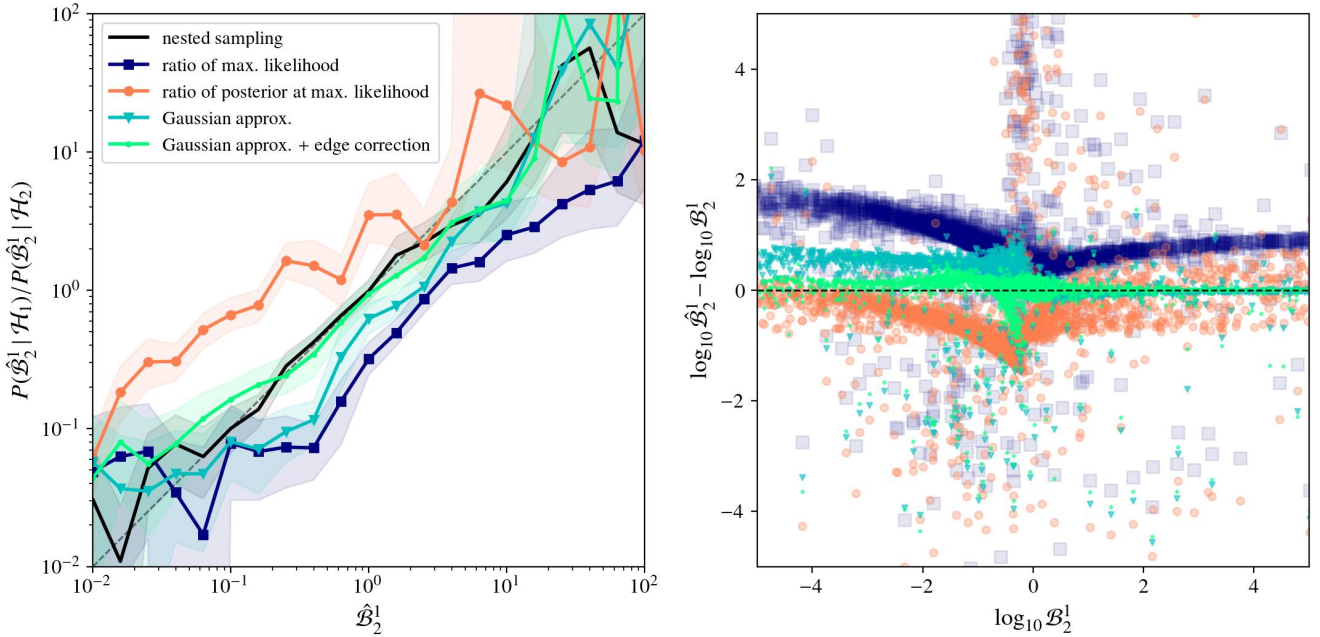


FIG. 1. Left: the BB plots for (numerically) exact nested sampling based Bayes factor between the alternative to GR and GR hypotheses in our toy problem, along with those corresponding to various approximations described in Eqs. (14), (15), (16), and (17). Shaded regions indicate 90% credible regions estimated assuming multinomial histogram errors. Right: difference between approximate and exact Bayes factor calculations plotted against the latter, for the four estimates discussed in the left-hand panel.

take hundreds to thousands of CPU hours. It is worth exploring whether simple approximations can be made to reduce these costs, and whether those approximations can be validated without ever computing the full nested sampling based \mathcal{B}_2^1 .

Therefore, in the beginning, we will assume that even for the simple problem posed above, it is impossible to sample the posteriors, compute the evidences, and calculate the \mathcal{B}_2^1 in a brute force manner. We will assume, however, that it is still possible to find the parameter vectors $\bar{\theta}_1^{\text{ML}}$ and $\bar{\theta}_2^{\text{ML}}$ corresponding to the maximum likelihood of the two models, and the Fisher covariance matrices [23] Σ_1 and Σ_2 around those locations. At low SNRs, this may be challenging as the posterior may be significantly non-Gaussian and possibly multimodal in the usual physical parameter space. However, clever reparameterization (such as that proposed in [24]) may simplify the posterior shape enough to obtain these quantities with relatively few likelihood evaluations.

The program is as follows: we simulate 3000 random realizations of data from each of the AG and GR models. On each sample strain, we evaluate our approximation $\hat{\mathcal{B}}_2^1$ of the Bayes factor. With these $\hat{\mathcal{B}}_2^1$ samples, we empirically reconstruct $P(\hat{\mathcal{B}}_2^1 | \mathcal{H}_1)$ and $P(\hat{\mathcal{B}}_2^1 | \mathcal{H}_2)$ and make a BB plot. If it lies close to equality, we deem the approximation valid; else, we improve upon it with additional terms.

We consider four approximations for the Bayes factor

1. Ratio of maximum likelihoods

$$\hat{\mathcal{B}}_2^1 = \frac{P(d | \bar{\theta}_1^{\text{ML}})}{P(d | \bar{\theta}_2^{\text{ML}})}. \quad (14)$$

2. Ratio of posteriors at maximum likelihood points

$$\hat{\mathcal{B}}_2^1 = \frac{P(d | \bar{\theta}_1^{\text{ML}}) P(\bar{\theta}_1^{\text{ML}} | \mathcal{H}_1)}{P(d | \bar{\theta}_2^{\text{ML}}) P(\bar{\theta}_2^{\text{ML}} | \mathcal{H}_2)}. \quad (15)$$

3. Gaussian approximation (also known as Laplace's approximation)

$$\hat{\mathcal{B}}_2^1 = \sqrt{2\pi} \frac{P(d | \bar{\theta}_1^{\text{ML}}) P(\bar{\theta}_1^{\text{ML}} | \mathcal{H}_1) |\Sigma_1|^{1/2}}{P(d | \bar{\theta}_2^{\text{ML}}) P(\bar{\theta}_2^{\text{ML}} | \mathcal{H}_2) |\Sigma_2|^{1/2}}. \quad (16)$$

4. Gaussian approximation with edge corrections

$$\hat{\mathcal{B}}_2^1 = \sqrt{2\pi} \frac{P(d | \bar{\theta}_1^{\text{ML}}) |\Sigma_1|^{1/2}}{P(d | \bar{\theta}_2^{\text{ML}}) |\Sigma_2|^{1/2}} \times \frac{\langle P(\bar{\theta}_{1,k} | \mathcal{H}_1) \rangle_{\bar{\theta}_{1,k} \sim G_1} f_1}{\langle P(\bar{\theta}_{2,k} | \mathcal{H}_2) \rangle_{\bar{\theta}_{2,k} \sim G_2} f_2}. \quad (17)$$

where, for $i \in \{1, 2\}$, G_i are multivariate Gaussians with mean $\bar{\theta}_i^{\text{ML}}$ and covariance Σ_i , $\bar{\theta}_{i,k}$ are samples from these Gaussians, and f_i is the fraction of those samples that lie within the prior boundaries.

The first two do not resemble expressions of the exact Bayes factor at all, and are chosen to illustrate how such bad approximations may be identified. The latter two are based on the Gaussian approximation and should therefore be treated with more importance.

The BB plots for these approximations are shown in the left-hand panel of Fig. 1. By checking whether the ratio $P(\mathcal{B}_2^1 | \mathcal{H}_1)/P(\mathcal{B}_2^1 | \mathcal{H}_2)$ lies above or below the equality line, we can infer that the likelihood ratio is an overestimate, while the posterior ratio is an underestimate. This is expected since they fail to account for the three main constituents of the Bayesian evidence: the likelihood, times the posterior, and their integration over the appropriate region of parameter space. The Gaussian approximation takes these into account and therefore gives a less biased BB plot. Accounting for edge effects further improves the Gaussian approximation, removing all the remaining bias. It may therefore be a viable alternative to expensive nested sampling-based Bayes factor calculation.

While future work can apply the above approximation in more realistic studies of gravitational waveform distortion, the key takeaway of the above exercise is that we arrived at this result *without* having to compare it against nested sampling. Equation (4) acts as a consistency test by itself, and as long as we can simulate data from the priors, we can use BB plots as a diagnostic tool to assess the accuracy of Bayes factor calculations without requiring access to the ground truth.

For completeness, we also compute the (numerically) exact Bayes factor using the NAUTILUS [22] nested sampler. The left-hand panel of Fig. 1 shows that its BB plot lies over the diagonal equality line, as expected. More importantly, as shown in the right-hand panel, the nature (i.e., over- or underestimation) of residuals between it and the approximations discussed above also matches what we had inferred using their BB plots.

B. Strong Gravitational Lensing of Gravitational Waves

In our second demonstration of the use of BB plots as a diagnostic tool, we describe our success at improving a Bayesian search pipeline for strongly lensed GWs.

Strong gravitational lensing of GWs occurs when a massive object (for eg, a galaxy) lies along our line-of-sight to a GW source (for eg, a binary black hole (BBH)). The gravity of the massive object (i.e., the “lens”) bends the paths of the GWs, potentially resulting in multiple—nearly identical—copies of the same source waveform reaching our detectors at different times. Except in very rare cases, the only way to detect them is by confidently identifying pairs of signals that resemble each other to such a degree that random chance alone cannot explain it [25].

The Bayes factor between the lensed and unlensed hy-

potheses is schematically given by [26–32]

$$\mathcal{B}_2^1 = \frac{\int d\vec{\theta}_1 P(d_A, d_B | \vec{\theta}_1) P(\vec{\theta}_1 | \mathcal{H}_1)}{\prod_{j \in \{A, B\}} \int d\vec{\theta}_2 P(d_j | \vec{\theta}_2) P(\vec{\theta}_2 | \mathcal{H}_2)} \quad (18)$$

where d_A, d_B are the data corresponding to the two individual signals, $\vec{\theta}_1$ and $\vec{\theta}_2$ parameterize the lensed and unlensed hypotheses \mathcal{H}_1 and \mathcal{H}_2 respectively. $\vec{\theta}_2$ are the usual BBH waveform parameters, while $\vec{\theta}_1$ additionally include lensing-related parameters such as magnification, phase shift, and time delay.

The Posterior Overlap 2.0 (hereafter, PO2.0) [31] formalism evaluates the above using the following approximation

$$P(d_A, d_B | \vec{\theta}_1) \propto P(\vec{\theta}_2 | d_A) \cdot P(\vec{\theta}_2 + \Delta\theta | d_B) \quad (19)$$

i.e., the joint likelihood is proportional (up to priors) to the product of the individual unlensed posteriors, with the second signal’s posterior evaluated at a location shifted by $\Delta\theta$ to account for the lensing magnification, phase shift, and time delay. The posterior distributions themselves are reconstructed from already available posterior samples using a density estimation algorithm, specifically, with `scipy’s gaussian_kde`.

Barsode et al. [16] made a BB plot for the PO2.0 \mathcal{B}_2^1 , and found that it was an underestimate by a factor of ~ 16 . Extensive code review revealed a few missing factors of 2 in the implementation, which were subsequently fixed. This highlights the potential of BB plots at identifying human errors.

Nevertheless, the corrected version of the code still showed a BB plot biased by ~ 2 (Fig. 5 of [16]). This was puzzling since the approximation made in Eq. (19) is expected to hold whenever the noise across different signals is uncorrelated (i.e., for non-overlapping signals), and when sub-dominant modes of gravitational radiation are weak or absent. Both of these conditions are satisfied by GW signals observable by the current generation of ground-based detectors, implying that the source of this factor of 2 was not theoretical, but numerical. Indeed, further analysis showed that this discrepancy ranged between a factor of 2 on *either side* of equality as we changed the bandwidth or the parameterization of the `gaussian_kde`, making it the likely culprit.

In high-dimensional distributions having non-linear correlations and multimodalities—such as those commonly observed in GW posteriors—density estimation is prone to biases. Kernel-based methods can be especially limited due to over- or undersmoothing, or “spillover” outside the prior boundaries. Recent machine learning techniques, such as normalizing flows, could potentially mitigate these issues by learning a series of invertible transformations between the given samples and a multivariate Gaussian distribution. A sufficiently deep network can fit GW posteriors with remarkable accuracy. Furthermore, once fit, these flows are quite inexpensive to evaluate and resample from.

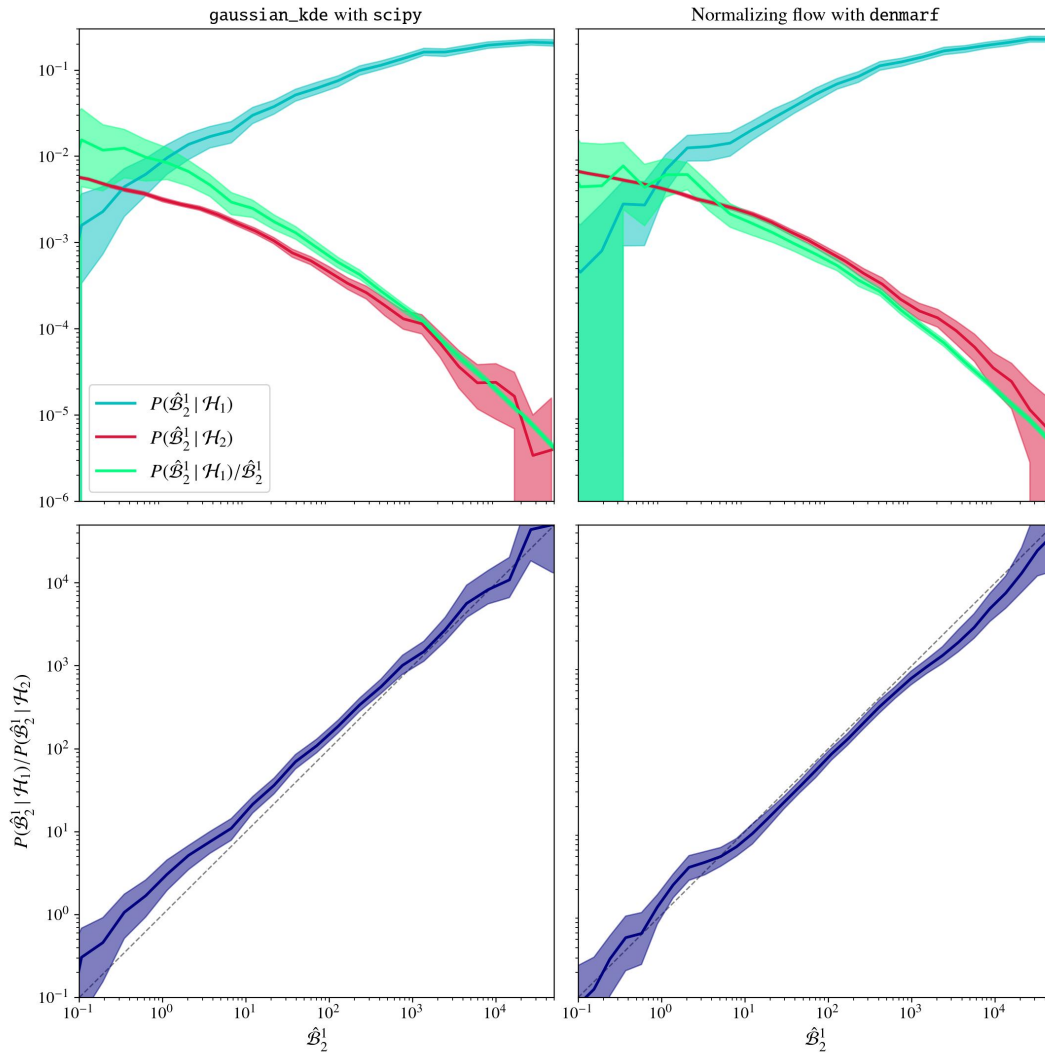


FIG. 2. The top row shows the probability distribution of the GW strong lensing Bayes factor \mathcal{B}_2^1 obtained using the PO2.0 method from a large number of simulated lensed and unlensed signals. Also plotted is $P(\mathcal{B}_2^1 | \mathcal{H}_1)$ scaled by \mathcal{B}_2^1 to show that it is very close to $P(\mathcal{B}_2^1 | \mathcal{H}_2)$. The same information is shown in the bottom row as *BB* plots. Shaded regions indicate 90% credible regions estimated assuming multinomial histogram errors. The left column shows results with the older `gaussian_kde` based approach, while the right column shows the same using the normalizing flow based implementation of PO2.0 \mathcal{B}_2^1 .

Thus, we present a new implementation of PO2.0 with a singular change: we replace `scipy` based `gaussian_kde` by a normalizing flow implementation `denmarf` [33]. We test it using simulated lensed and unlensed GW signals (see Appendix A for simulation details) and produce a *BB* plot. As Fig. 2 shows, the `denmarf` based implementation is indeed less biased than `gaussian_kde`. The remaining systematic uncertainty is now *below* the inherent statistical uncertainty due to a finite number of posterior samples (not shown in Fig. 2. See [31], and also Appendix A). Additional comparisons between the old and the new methods can be found in Appendix A.

We conclude that the new PO2.0 implementation computes the \mathcal{B}_2^1 with high accuracy, as backed by the *BB* plot. Furthermore, it is also about one to two orders

of magnitude less computationally expensive, marking a significant step towards detecting strongly lensed GWs within realistic computational budgets.

IV. ESTIMATING BACKGROUNDS

In the previous section, we demonstrated two examples for benchmarking the accuracy of Bayes factors using backgrounds and foregrounds. For some, these validated Bayes factors may be sufficient at their face value for model selection, while others may demand a comparison with a background distribution for estimating the statistical significance of that result.

In many realistic problems, background generation can

be highly computationally expensive. The purpose of this section is to illustrate the power of BB plots at estimating backgrounds at low computational costs. The implicit assumption here is that the Bayes factors are accurate and that all of our modeling assumptions are close to reality so that the BB relationship holds.

This is arguably rather idealistic to assume, and real observations will still demand a rigorous background simulation. However, a simple estimate of the statistical significance can be valuable for an initial assessment of an outlier, and it can be used to justify/reject detailed investigations. The methods outlined here may also be useful for validating search pipelines in regimes not directly accessible due to computational limitations, as well as for forecasting purposes.

We briefly note that while our main focus will be on background estimation, similar techniques can also be applied for estimating foregrounds. This may have some applications in hierarchical search pipelines (eg. [34]) for choosing intermediate thresholds, etc.

A. Background for Strong Lensing of GWs

Because the search for strongly lensed GWs must be performed over all possible pairs of signals in the catalog, the computational costs rise quadratically with the size of the catalog. The background needs to simulate roughly a few million *times* more pairs to enable establishing statistical significance up to 5σ . For the ~ 250 GW events detected so far [35], this is $\sim 10^{11}$ pairs, requiring about a year of computation on a large cluster to finish calculating \mathcal{B}_2^1 's using the PO2.0 method (see Sec. III B).

By the time when the first detection is likely to occur (the fifth observing run (O5) of LIGO-Virgo-KAGRA (LVK) [16]), the costs will be even higher, by about three to four orders of magnitude. Thus, with brute force becoming forbiddingly expensive, there is clear motivation to look for alternative ways to estimate the background distribution.

The crux of the problem is that while we need to probe the background at the high- \mathcal{B}_2^1 tail (where lensed events and false alarms would lie), by virtue of it *being* the tail, it is highly inefficient to sample from it using a brute force approach. The BB relationship provides a potential way to improve the sampling efficiency: we can simulate a *foreground* (which samples precisely the range of interesting \mathcal{B}_2^1 's), and convert it to a background through Eq. (4) [16].

The conversion can be done by dividing the empirically constructed (for eg, using a histogram) probability distribution $P(\mathcal{B}_2^1 | \mathcal{H}_1)$ by \mathcal{B}_2^1 . However, since samples of the lensed \mathcal{B}_2^1 's are available, the same can be achieved more robustly by reweighting each sample by its inverse,

leading to (pairwise) FPP

$$1 - C(\mathcal{B}_2^1 | \mathcal{H}_2) \approx \frac{1}{N_\ell} \sum_{k=1}^{N_\ell} \frac{\Theta(\mathcal{B}_{2k}^1 \geq \mathcal{B}_2^1)}{\mathcal{B}_{2k}^1} \quad (20)$$

where N_ℓ is the number of samples $\{\mathcal{B}_{2k}^1\}$ available from the foreground $P(\mathcal{B}_2^1 | \mathcal{H}_1)$ and Θ is the Heaviside step function. Figure 3 shows that, at current detector sensitivities, this approach can estimate FPPs accurate to within a factor of 2 using just 300 foreground simulations, to be contrasted against the $\sim 10^{11}$ simulations needed in the brute force approach.

1. A semi-empirical approach

Here, we show that it is possible to obtain a deep background semi-empirically, using a smaller background or foreground. The idea is as follows: there exist theoretical or empirically observed correlations between the foreground Bayes factor and certain properties of the signals (for eg, the SNR). It is easy to obtain the distribution of these properties using theoretical arguments or simulations, using which one can marginalize over them to obtain the foreground distribution of the Bayes factor. The BB relationship is then used to transform it to the background distribution. There may be unknown parameters describing such backgrounds, which need to be estimated by fitting with a few simulations.

In the case of strong lensing of GWs, Barsode et al. [16] showed that lensed \mathcal{B}_2^1 are correlated with a particular combination of SNRs ρ_1, ρ_2 of the two lensed images

$$\log_{10} \mathcal{B}_2^1 = D \log_{10} \rho + \mathcal{N}(\mu, \sigma) \quad (21)$$

where D is the effective dimensionality of the posterior distributions of individual signals, $\mathcal{N}(\mu, \sigma)$ describes (log) Gaussian uncertainty with mean μ (not to be confused with lensing magnification) and standard deviation σ ,¹ and $\rho = \sqrt{2\rho_A^2\rho_B^2/(\rho_A^2 + \rho_B^2)}$.

In the local universe, homogeneity and isotropy would suggest that the distribution of ρ_A and ρ_B should be a power law with slope -4 above a detection threshold $\rho_{\text{th}} \sim 8$.² Strictly speaking, since the sources observable by the LVK are already at cosmological scales, this is not expected to be true. Further, ρ will be distributed differently from ρ_A or ρ_B even if the relative magnification is close to unity and $\rho_A \simeq \rho_B$. However, the deviation is expected to be small, and if desired, the exact distribution can be easily incorporated using astrophysical simulations.

¹ to be precise, the correlation in Eq. (21) as proposed by [16] excluded time delay information, but here we absorb it into the Gaussian uncertainty

² For a uniform density of GW sources, the distance d would be distributed as $\propto d^2$. Since $\rho \propto 1/d$, including the Jacobian $\propto \rho^{-2}$, we obtain $P(\rho) \propto \rho^{-4}$.

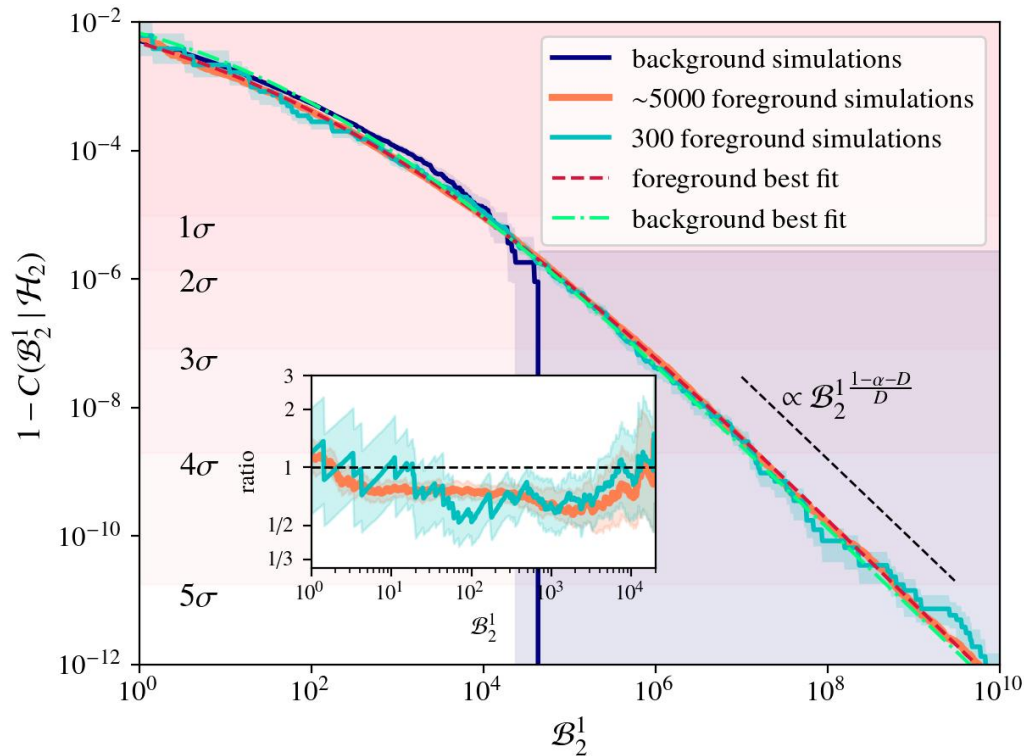


FIG. 3. The (pairwise) false positive probability (i.e., the survival function of the background) of the GW strong lensing Bayes factor. This is shown for ground truth background simulations, as well as for estimates made using foreground samples weighted according to the BB relationship, and semi-empirical fits to the foreground and background. Ratios of these estimates against the ground truth are shown in the inset, up to the region where the latter is valid. Shaded regions around the histograms indicate 90% credible regions estimated with bootstrapping, while pink shades indicate statistical significance σ thresholds in a catalog of 254 events. Dashed line indicates a power law behavior of the background, with power law index related to the slope α of the SNR distribution, as well as the effective dimensionality (D) of the posterior distributions (see Eq. (25)).

Here, as a simple model for demonstration, we consider ρ to be distributed as a power law with slope $-\alpha$ above ρ_{th} . Then, it is possible to marginalize Eq. (21) over ρ to obtain the foreground distribution in terms of $\alpha, \rho_{\text{th}}, D, \mu$ and σ

$$P(\log_{10} \mathcal{B}_2^1 | \mathcal{H}_1) = (\alpha - 1) \rho_{\text{th}}^{\alpha-1} \int_{\rho_{\text{th}}}^{\infty} d\rho \rho^{-\alpha} \times \mathcal{N}(\mu + D \log_{10} \rho - \log_{10} \mathcal{B}_2^1, \sigma). \quad (22)$$

This can be integrated analytically, resulting in

$$P(\log_{10} \mathcal{B}_2^1 | \mathcal{H}_1) = \frac{1}{2} \beta \rho_{\text{th}}^{\alpha-1} e^{\beta \mu + \frac{1}{2} \beta^2 \sigma^2} \mathcal{B}_2^1 \frac{1-\alpha}{D} \times \left(1 - \text{erf} \left(\frac{\beta \sigma}{\sqrt{2}} + \frac{\mu + D \log_{10} \rho_{\text{th}} - \log_{10} \mathcal{B}_2^1}{\sqrt{2} \sigma} \right) \right) \quad (23)$$

where $\beta = \log 10 \times (\alpha - 1)/D$. The background is then given by the BB relationship (Eq. (4), with an extra $1/\mathcal{B}_2^1$ Jacobian to transform from $P(\log_{10} \mathcal{B}_2^1)$ to $P(\mathcal{B}_2^1)$)

$$P(\mathcal{B}_2^1 | \mathcal{H}_2) = \frac{P(\log_{10} \mathcal{B}_2^1 | \mathcal{H}_1)}{\mathcal{B}_2^{1/2}}. \quad (24)$$

At large \mathcal{B}_2^1 , the erf term is insignificant, implying that the background, and consequently the FPP in strong GW lensing, is a power law in \mathcal{B}_2^1

$$1 - C(\mathcal{B}_2^1 | \mathcal{H}_2) \propto \mathcal{B}_2^{1 \frac{1-\alpha-D}{D}}. \quad (25)$$

While these formulae are completely analytical, the parameters $\alpha, \rho_{\text{th}}, D, \mu, \sigma$ must be anchored to data by fitting Eq. (23) to available foreground, or Eq. (24) to available background. The latter is a significant result: it lets us take a limited background and extrapolate it without running any extra simulations.

For the PO2.0 data from Sec. IIIB and Appendix A, we find the best fit $[\alpha, \rho_{\text{th}}, D, \mu, \sigma]$ to be $[3.7, 8.2, 8.9, -4.6, 1.5]$ for the foreground, and $[3.5, 8.0, 9.0, -5.0, 1.4]$ for the background. The analytical FPP vs \mathcal{B}_2^1 curves corresponding to these best fit parameters are shown in Fig. 3 and match within a factor of 2 with the brute force background, and quite closely with the sampling-based background obtained from foreground using Eq. (20).

B. The Lensing Interpretation of GW231123

GW231123 was identified by the LVK [36] as an outlier with a Bayes factor $\sim 10^4$ in favor of it being a signal with a waveform modified due to lensing in the wave-optics regime. If GW231123 is indeed lensed, establishing 5σ statistical significance would require $\gtrsim 10^8$ background simulations³. However, with only 254 simulations in their computationally limited background, the LVK could only put a lower bound of $\sim 1\sigma$. While non-lensing explanations such as overlapping signals [37] or a merger of primordial black holes [38, 39] have been proposed, a number of lensing studies have also followed [40–44]. Chan et al. [41], in particular, used simulation-based inference to generate a deep, brute-force background to establish an upper bound of $\sim 4\sigma$.

Here, we will obtain the same result, but instead of running a large number of simulations, we will extrapolate LVK’s limited astrophysical background using a semi-empirical approach based on the BB relationship similar to that shown in the previous subsection. Since this implicitly assumes stationary Gaussian noise, our answer will only be a rough, order-of-magnitude estimate.

First, we need a prescription for the foreground. We use the “fitting factor” approximation given by [18, 45, 46]. The expectation is that, in the high-SNR limit, the logarithm of the Bayes factor increases quadratically with the SNR ρ . Its coefficient is related to a “fitting factor” $FF \in [0, 1]$ that quantifies how well an unlensed waveform can match a lensed waveform. Including another term proportional to $\log FF$ [46] and a $\sim \rho\sqrt{2(1-FF)}$ Gaussian fluctuation [45], this becomes

$$\log \mathcal{B}_2^1(\rho, FF) \simeq \frac{1}{2}(1 - FF^2)\rho^2 + (D - d) \log FF + d \log \rho - \mathcal{O} + \mathcal{N}\left(0, \rho\sqrt{2(1 - FF)}\right) \quad (26)$$

where D is the number of parameters that we can effectively measure from unlensed signals, d is the number of additional parameters required for describing the lensed signal, and $\mathcal{N}(\mu, \sigma)$ denotes Gaussian uncertainty with mean μ and standard deviation σ . \mathcal{O} is the Bayesian Occam factor that quantifies the reduction in the prior volume of the additional parameters due to the information in the data. In general, the measurement uncertainties in each parameter reduce roughly in proportion to ρ . We have factorized that $d \log \rho$ dependence out of the Occam factor, making \mathcal{O} roughly constant for a given problem.

Since we are only interested in a rough estimate, we simplify the above even further by effectively marginalizing over the unknown distribution of FF . We assume that the \log_{10} Bayes factor is distributed around a mean function $f\rho^2 + d \log \rho - \mathcal{O}$, with uncertainties due to those

in FF absorbed by an effective standard deviation of the Gaussian

$$\log_{10} \mathcal{B}_2^1(\rho) \simeq f\rho^2 + d \log_{10} \rho - \mathcal{O} + \mathcal{N}(0, s_0 + s_1\rho + s_2\rho^2). \quad (27)$$

Following similar steps as in the previous subsection, we assume a power law distribution for ρ with slope $-\alpha$ above a threshold ρ_{th} , and numerically marginalize over ρ . This results in a semi-empirical foreground distribution, which can then be converted to a background using the BB relationship (Eq. (4) or (24)).

	distribution	minimum	maximum
f	LogUniform	10^{-8}	0.5
α	Uniform	3	5
ρ_{th}	Uniform	7	9
\mathcal{O}	Uniform	-10	10
d	Uniform	0	3
s_0	LogUniform	10^{-6}	1
s_1	LogUniform	10^{-6}	1
s_2	LogUniform	10^{-6}	1

TABLE I. Priors used in fitting unknown parameters of our semi-empirical model to LVK’s limited background for wave-optics lensing distortion.

We constrain the free parameters $f, \alpha, \rho_{\text{th}}, d, \mathcal{O}, s_0, s_1, s_2$ by fitting our semi-empirical model to LVK’s background sample of 254 simulations. Our chosen priors for this analysis are listed in Tab. IV B. The resulting range of possible backgrounds is shown in Fig. 4. Nominally, we find that GW231123 is a 4.1–4.5 σ significant candidate for wave-optics lensing.

To check the robustness of these fits, we experimented with prior ranges different from those listed in Tab. IV B, as well as with fits where one or two of s_0, s_1, s_2 were fixed at 0. Some of these choices extended possible backgrounds down to slightly lower FPPs, though the estimated statistical significance remains $\gtrsim 4.1\sigma$. Further validation of this methodology is presented in Appendix B.

A confident interpretation—lensing or otherwise—is hampered by the presence of severe waveform systematics [17, 41, 47] and probable noise transients within the event’s strain [47–49], both of which are outside the scope of a BB plot based background estimate. The BB plot assumes stationary Gaussian noise (same as the likelihood used in the computation of evidences), while background injections in real noise are prone to non-stationarities as well as non-Gaussianities. These could result in the *real* background having heavier tails than our Gaussian expectation [50]. This is perhaps visible in our fits: while they remain consistently within errorbars of the real tail, they appear to lie on the lower side.

Thus, our estimate of the statistical significance should be treated as an upper bound of 4.1σ . This is consistent with that estimated by [41] using a detailed study, though we remark that their background was not distributed ac-

³ including the trials factor corresponding to 84 events in O4a

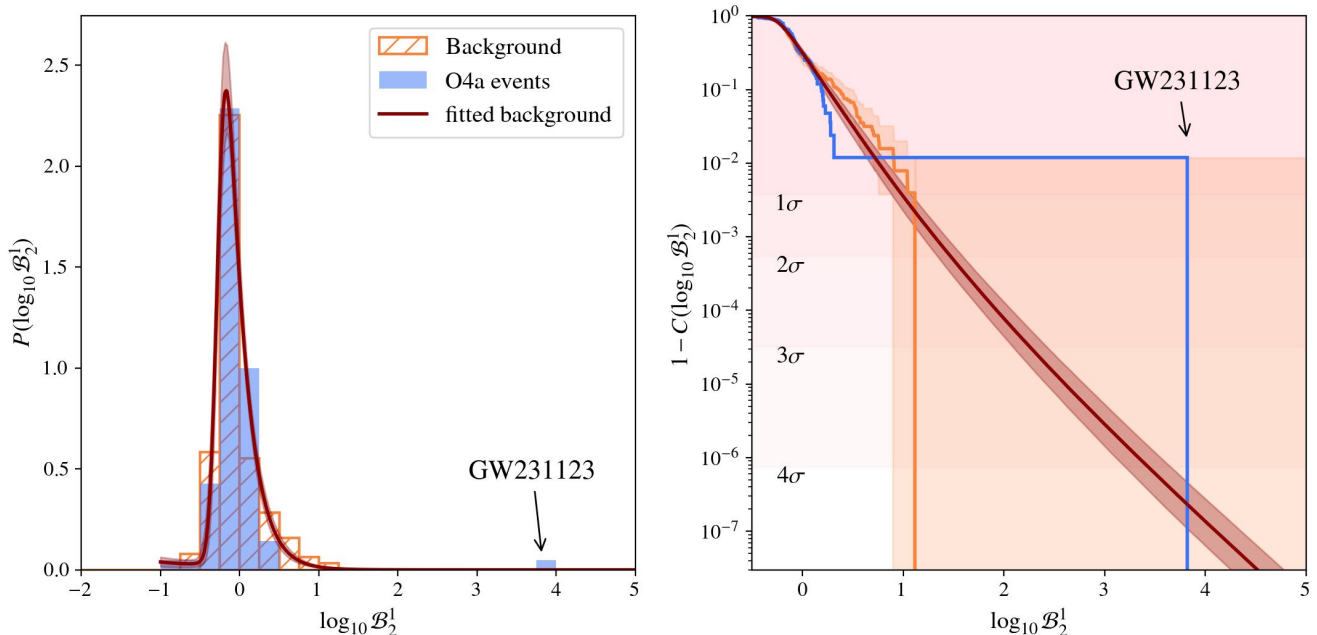


FIG. 4. Left: histograms of wave-optics lensing Bayes factors for O4a events and background simulations as published by the LVK. Also plotted is our range of possible semi-empirical backgrounds in dark red. Right: The (eventwise) false positive probability (i.e., the survival function of the background distribution), along with a survival function of the observed events, and our semi-empirical extrapolation to the background. Orange shaded regions show 90% credible regions estimated with bootstrapping, while pink shades indicate statistical significance σ thresholds in a catalog of 84 events.

ording to astrophysical priors, and it did not include the catalog trials factor of ~ 84 .

For more impactful estimates of the statistical significance, some improvements would be desirable in our semi-empirical background model (Eq. (27)). For instance, we can use simulated distributions of fitting factors and SNRs for marginalization, or the Gaussian noise term could be substituted with a heavier-tailed distribution to model the low-FPP region more accurately. We would also need to include selection effects due to the initial matched filtering step that is usually performed without taking waveform distortion into account [51]. Importantly, these estimates would need calibration against at least a limited but real background. We leave these as future work.

V. CONCLUSION

Bayes factors are foundational to many scientific discoveries in the modern era. Yet, due to computational complexity, the practical implementation of Bayes factor calculation may be only approximate. There is also a possibility of human error, resulting in potentially biased estimates.

In this paper, we have described the Bayes factor-Bayes factor or *BB* plot to assess the accuracy of such implementations without requiring access to the ground truth.

Guided by *BB* plots, we improved the PO2.0 method for searching strongly lensed GWs, with the new implementation being both accurate and more computationally efficient. It may be instrumental in realizing the detection of lensed multiple images anticipated in the upcoming years, especially in the face of large catalog sizes.

Using the *BB* plot, we also showed that it is possible to detect gravitational waveform distortion using fast Fisher covariance matrix-based Bayes factors. Here, we used a toy model for demonstration, but we are currently working on applying these methods in realistic searches for wave-optics and saddle-point lensing of GWs, tests of GR, orbital eccentricity, and environmental effects.

We note that the *BB* plots offer a necessary consistency test, but they are not sufficient. Arbitrary likelihood ratios may satisfy them, though we believe this should be easily recognizable in the practical implementation. Further work may focus on removing this caveat with help from other simulation-based validation methods proposed in the literature [14, 15].

Beyond diagnostics, the *BB* relationship can also be used to estimate frequentist style backgrounds using the Bayes factor as the optimal statistic. We derived an analytical expression for the background of GW strong lensing, and showed that it can estimate FPPs within a factor of 2 of the ground truth. Being analytical, these backgrounds can be easily extrapolated to FPPs that are unreachable by brute force simulations. Using

a similar approach but in the wave-optics regime of lensing, we also derived a semi-numerical extrapolation for the background in GWTC4, and used it to estimate a rough bound on the statistical significance of GW231123 at $\lesssim 4.1\sigma$, assuming Gaussian noise.

These semi-empirical background-foreground models open a rather intriguing possibility⁴: we may fit the distribution of real events' Bayes factors with a mixture of background and foreground models. The mixture coefficient can be estimated from the real data itself, resulting in bounds on the presence and statistical significance of outliers without requiring any simulations. Future work would be to test how reliable such estimates are in comparison to rigorous studies.

While the statistical significance of an observed candidate will ultimately be decided by rigorous background simulations regardless of the computational costs, the rough bound estimated with our approach is still valuable for an initial assessment of outliers similar to GW231123. Furthermore, these techniques will certainly be useful in the development of search pipelines and in making forecasts.

The applications discussed here were limited to GW astronomy, however *BB* plots are quite general and could be useful in any field that relies on model selection with Bayes factors. While their effectiveness depends on the accuracy of the underlying statistical assumptions, they offer a simple and computationally efficient tool for both validating Bayes factor calculations and estimating statistical significance. We anticipate that these methods will find broader use in large-scale inference problems where exact calculations are impractical.

ACKNOWLEDGMENTS

I thank Juno Chan for graciously providing data from their work on DINGO-LENSING [41, 52]. I also thank Mick Wright, Ajith Parameswaran, and Anjali Bhattar for a careful review of this manuscript. I acknowledge support from Koustav N. Maity, Siva Athreya, Otto A. Hannuksela, Rico Lo, V Sree Suswara, and Dootika Vats. I also thank members of the astrophysical relativity group at ICTS and the LVK Lensing group for constructive feedback on this work. My research is supported by the Department of Atomic Energy, Government of India, under Project Nos. RTI4019 and RTI4013. The numerical calculations reported in the paper were performed on the Alice computing cluster at ICTS-TIFR.

This work makes use of the `cogwheel` [24, 53], `scipy` [54], and `nautilus` [22] software packages. This material is based upon work supported by NSF's LIGO Laboratory, which is a major facility fully funded by the National Science Foundation.

⁴ partially credited to Otto A. Hannuksela

DATA AVAILABILITY

The data and code used in this study are available from the author upon reasonable request.

Appendix A: GW strong lensing search using PO2.0

Here, we outline the methodology used for generating simulated unlensed and strongly lensed GW signals on which we test our implementation of PO2.0. We also provide additional comparison plots between the old and the new implementation.

Our astrophysical simulation is identical to that from [31], though we use the latest available data regarding the GW populations. We generate an intrinsic population of GW sources according to the population inferred from observed BBHs at the end of the first part of the fourth observing run of the LVK [55], with a merger rate following the star formation rate [56]. Depending on the optical depth of strong lensing to the GW source's redshift, they are assigned galaxy lenses distributed according to the SDSS catalog [57] with a Singular Isothermal Ellipsoid [58, 59] profile. Their detectability is assessed by thresholding the optimal SNR at 8, where the SNR is computed at the projected sensitivity corresponding to the fourth observing run (O4) of the LVK [60], assuming a 2.5 year observing duration and ignoring detector down times, using the IMRPHENOMXPHM [61] waveform model.

With the detectable populations generated as above, 1500 unlensed and 5000 lensed pairs of waveforms are injected in colored Gaussian noise corresponding to the same O4 sensitivity. The effect of Morse phase shift [21] is included by multiplying the waveforms of saddle point lensed images by $e^{i\pi/2}$. Parameter estimation on these mock strains is performed with the COGWHEEL [24, 53] package, generating the common dataset on which both the implementations of PO2.0 are tested.

Figure 5 shows a comparison of the Bayes factors computed by the two approaches for the same pairs of signals. The left-hand plot shows that the old and the new \mathcal{B}_2^1 's are tightly correlated for lensed pairs. The right-hand panel shows that the residuals follow the expected sampling error budget of ~ 0.3 in $\log_{10} \mathcal{B}_2^1$ (with a factor of $\sqrt{2}$ to account for the error in individual calculation), though with a small shift and skew, signifying a non-trivial change brought in by the new method. For unlensed pairs, there is a relatively large scatter between the \mathcal{B}_2^1 's computed with the two methods, and it does not follow the estimated error budget. However, since lensing search focuses entirely on the high \mathcal{B}_2^1 regime, this does not concern us.

The accuracy of unlensed pairs' Bayes factors *is* important for false alarms, i.e., unlensed pairs that accidentally result in high \mathcal{B}_2^1 's. This is best assessed with Receiver Operating Characteristics (ROC) plots, showing the efficiency (i.e., the true positive probability) against the

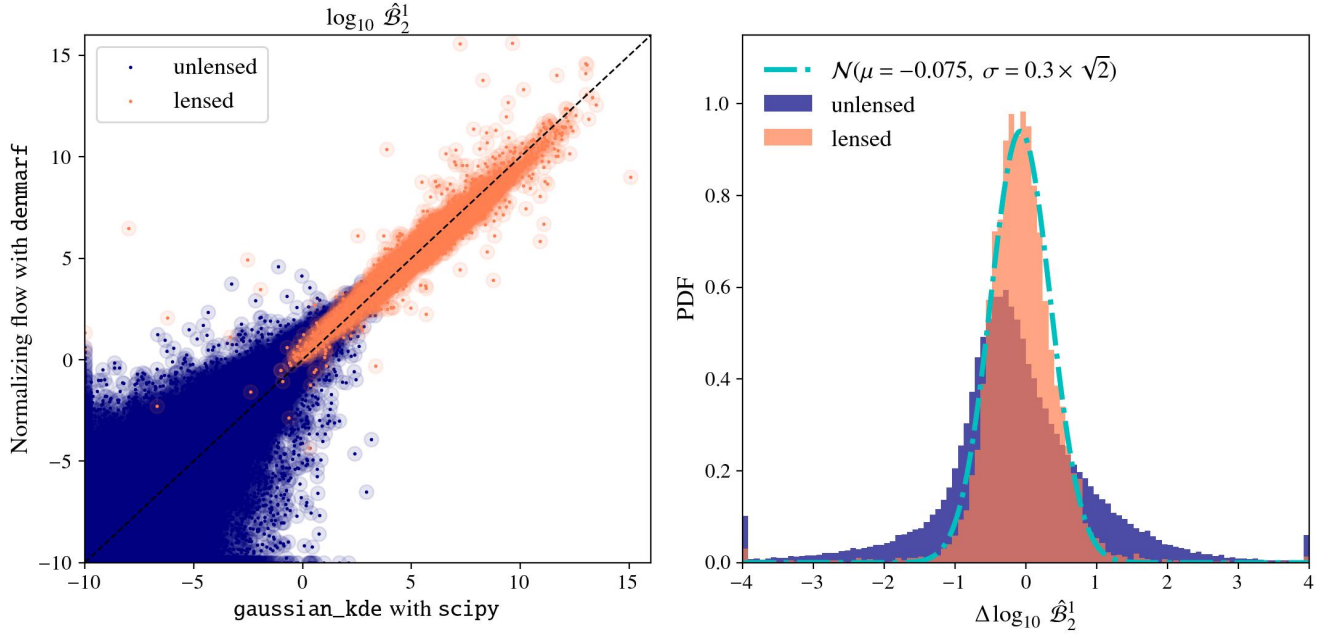


FIG. 5. Left: the new PO2.0 Bayes factors plotted against the old, both being computed on the same dataset. Faint disks denote 1 standard deviation of statistical uncertainty. Right: histogram of the difference between the new and old implementation. Also plotted is a Gaussian distribution with mean given by the median of the differences between lensed Bayes factors, and a standard deviation estimated using a statistical sampling uncertainty of 0.3 in each measurement [31].

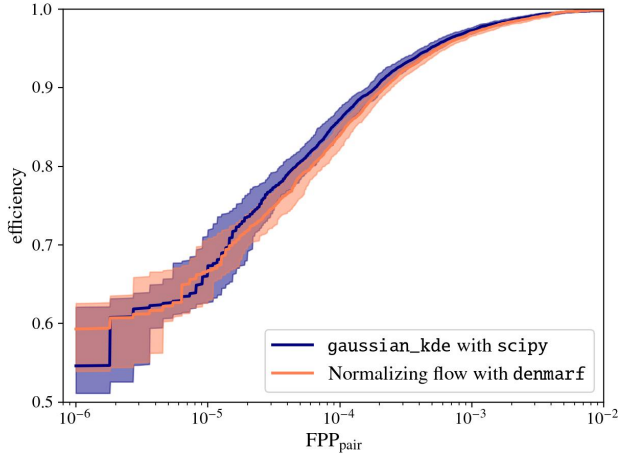


FIG. 6. The efficiency (i.e., the true positive probability) of finding strongly lensed GWs as a function of the (pairwise) FPP for the old and new implementations of PO2.0. Shaded regions show 90% credible regions estimated using bootstrapping.

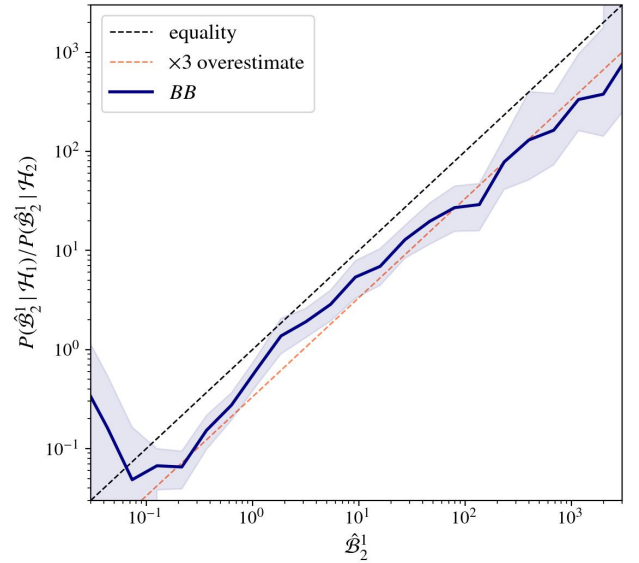


FIG. 7. The *BB* plot made for DINGO-LENSING Bayes factors made using data from [41] for the NRSUR7DQ4 waveform model. Shaded regions indicate 90% credible regions estimated assuming multinomial histogram errors.

(pairwise) FPP. Figure 6 shows that the old and new methods agree to within the expected sampling error budget.

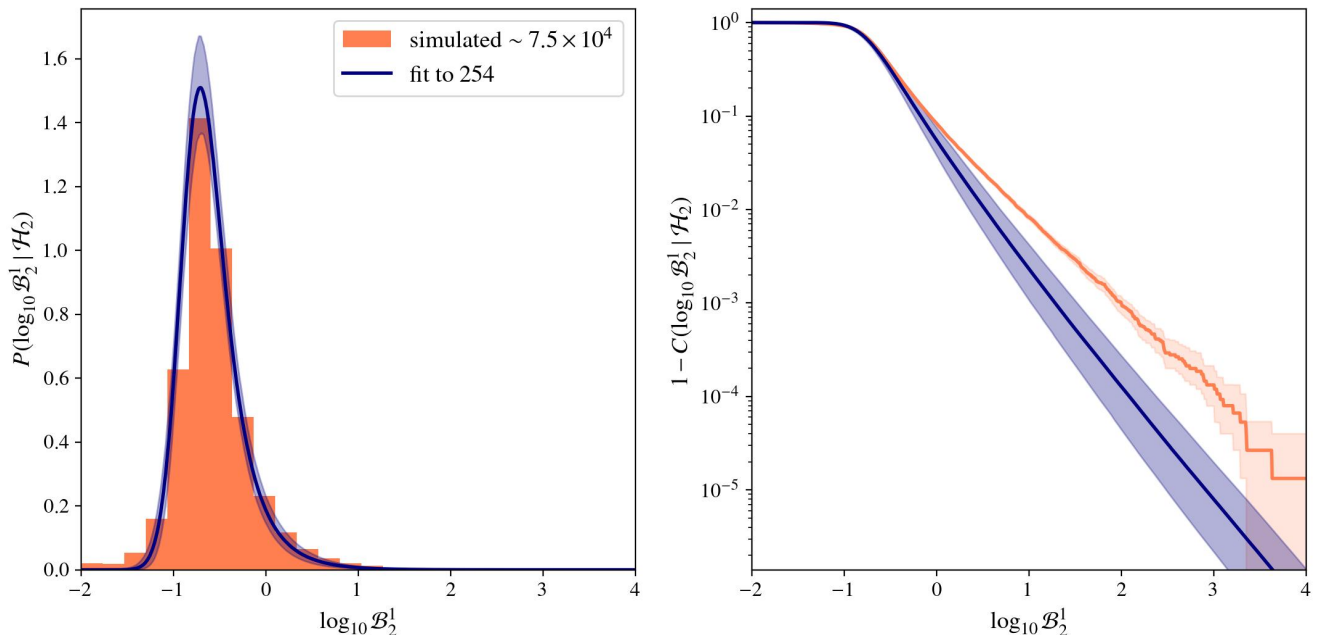


FIG. 8. Histogram (left) and reversed cumulative distribution (right) for DINGO-LENSING Bayes factors from [41] for the NRSUR7DQ4 waveform model. Also plotted is a semi-empirical fit based on Eq. (27) to a smaller sample of 254 to show that the extrapolation bounds the cumulative distribution from below. Shaded regions indicate 90% credible regions.

Appendix B: Validating dingo-lensing and Background Estimation

Chan et al. [41, 52] developed a neural posterior estimation framework called DINGO-LENSING for studying lensing of gravitational waves. This code drastically reduces the computational cost of computing lensing Bayes factors, making it possible to generate foregrounds and backgrounds within realistic computational budgets.

In particular, Chan et al. produced a background and foreground for GW231123-like signals using the NRSUR7DQ4 waveform model, shown in Fig. 4 of [41]. Using the original data provided by them, we show a BB plot in Fig. 7, finding a systematic deviation from the BB relation by a factor of ~ 3 . This is larger than the statistical fluctuation of $\sim 0.7 - 1.4$ they find when compared against nested sampling using BILBY. The higher systematic deviation is likely caused by a mismatch in the priors used for drawing the injection parameters and those used for evaluating the Bayes factors (the latter being broader than the former), which breaks one of the requirements

of making the BB plot. We emphasize that this *does not alter their conclusions in [41]*, since they were made using frequentist estimates that are robust against such mismatches.

We next test whether our semi-empirical formulation (in particular, Eq. (27)) for the background of waveform distortion effects matches Chan et al’s distributions, or at least bounds the FPPs from below. Since the BB plot is sensitive to waveform systematics, we restrict this test to NRSUR7DQ4, which is the most appropriate among the available waveform models in the parameter range surrounding GW231123 [17]. Note that the above-mentioned bias would not affect this fit; it simply gets absorbed in the free parameter \mathcal{O} .

We draw 254 random samples from their background Bayes factors, fit them with the semi-empirical procedure described in Sec. IV B⁵, and plot its extrapolation alongside the cumulative histogram obtained from the full dataset of $\sim 7.5 \times 10^4$. As Fig. 8 shows, the semi-empirical fit provides a consistent lower bound, validating the results in Sec. IV B.

⁵ with priors same as those in Tab. IV B except for a more relaxed prior for $\alpha \in [1, 5]$

-
- [1] B. P. Abbott, R. Abbott, T. D. Abbott, M. R. Abernathy, F. Acernese, K. Ackley, C. Adams, T. Adams, P. Addesso, R. X. Adhikari, *et al.*, Observation of gravitational waves from a binary black hole merger, Physical review letters **116**, 061102 (2016).
 - [2] C. Collaboration *et al.*, Observation of a new boson at

- a mass of 125 gev with the cms experiment at the lhc, arXiv preprint arXiv:1207.7235 (2012).
- [3] B. P. Abbott, R. Abbott, T. D. Abbott, F. Acernese, K. Ackley, C. Adams, T. Adams, P. Addesso, R. X. Adhikari, V. B. Adya, *et al.*, Gw170817: observation of gravitational waves from a binary neutron star inspiral, *Physical review letters* **119**, 161101 (2017).
 - [4] W.-W. Yu and B. Allen, Stochastic gravitational-wave background search using data from five pulsar timing arrays, arXiv preprint arXiv:2512.08666 (2025).
 - [5] A. G. Riess, A. V. Filippenko, P. Challis, A. Clocchiatti, A. Diercks, P. M. Garnavich, R. L. Gilliland, C. J. Hogan, S. Jha, R. P. Kirshner, *et al.*, Observational evidence from supernovae for an accelerating universe and a cosmological constant, *The astronomical journal* **116**, 1009 (1998).
 - [6] A. Adame, J. Aguilar, S. Ahlen, S. Alam, D. Alexander, M. Alvarez, O. Alves, A. Anand, U. Andrade, E. Armengaud, *et al.*, Desi 2024 vi: cosmological constraints from the measurements of baryon acoustic oscillations, *Journal of Cosmology and Astroparticle Physics* **2025** (02), 021.
 - [7] H. Jeffreys, *Theory of probability, with corrections* (1939).
 - [8] J. Neyman and E. S. Pearson, Ix. on the problem of the most efficient tests of statistical hypotheses, *Philosophical Transactions of the Royal Society of London. Series A, Containing Papers of a Mathematical or Physical Character* **231**, 289 (1933).
 - [9] J. Skilling, *Nested sampling for general bayesian computation*, (2006).
 - [10] D. Sivia and J. Skilling, *Data analysis: a Bayesian tutorial* (OUP Oxford, 2006).
 - [11] I. J. Good, A list of properties of bayes-turing factors, *NSA Technical Journal* **10**, 1 (1965).
 - [12] N. Sekulovski, M. Marsman, and E.-J. Wagenmakers, A good check on the bayes factor, *Behavior Research Methods* **56**, 8552 (2024).
 - [13] K. Okada, Optimality of the half-order exponent in the turing-good identities for bayes factors, arXiv preprint arXiv:2602.19838 (2026).
 - [14] M. Modrák, A. H. Moon, S. Kim, P. Bürkner, N. Huurre, K. Faltejsková, A. Gelman, and A. Vehtari, Simulation-based calibration checking for bayesian computation: The choice of test quantities shapes sensitivity, *Bayesian Analysis* **20**, 461 (2023).
 - [15] M. Modrák, S. Stoppel, and P.-C. Bürkner, Simulation-based validation of bayes factor computation, arXiv preprint arXiv:2508.11814 (2025).
 - [16] A. Barsode, K. Maity, and P. Ajith, Lensing, not luck! detection prospects of strongly lensed gravitational waves, *ApJ* **998**, 294 (2026), arXiv:2510.23238 [gr-qc].
 - [17] A. Abac, I. Abouelfettouh, F. Acernese, K. Ackley, C. Adamcewicz, S. Adhichary, D. Adhikari, N. Adhikari, R. Adhikari, V. Adkins, *et al.*, Gw231123: a binary black hole merger with total mass 190–265 msun, *The Astrophysical Journal Letters* **993**, L25 (2025).
 - [18] N. Cornish, L. Sampson, N. Yunes, and F. Pretorius, Gravitational wave tests of general relativity with the parameterizedj? format?; post-einsteinian framework, *Physical Review D—Particles, Fields, Gravitation, and Cosmology* **84**, 062003 (2011).
 - [19] J. Lawrence, Focusing of gravitational radiation by interior gravitational fields, *Il Nuovo Cimento B* (1971-1996) **6**, 225 (1971).
 - [20] R. Takahashi and T. Nakamura, Wave effects in the gravitational lensing of gravitational waves from chirping binaries, *ApJ* **595**, 1039 (2003).
 - [21] L. Dai and T. Venumadhav, On the waveforms of gravitationally lensed gravitational waves, arXiv preprint arXiv:1702.04724 (2017).
 - [22] J. U. Lange, nautilus: boosting Bayesian importance nested sampling with deep learning, *Monthly Notices of the Royal Astronomical Society* **525**, 3181 (2023), <https://academic.oup.com/mnras/article-pdf/525/2/3181/51331635/stad2441.pdf>.
 - [23] C. Cutler and E. E. Flanagan, Gravitational waves from merging compact binaries: How accurately can one extract the binary’s parameters from the inspiral waveform?, *PRD* **49**, 2658 (1994).
 - [24] J. Roulet, S. Olsen, J. Mushkin, T. Islam, T. Venumadhav, B. Zackay, and M. Zaldarriaga, Removing degeneracy and multimodality in gravitational wave source parameters, *PRD* **106**, 123015 (2022).
 - [25] K. Haris, A. K. Mehta, S. Kumar, T. Venumadhav, and P. Ajith, Identifying strongly lensed gravitational wave signals from binary black hole mergers, arXiv preprint arXiv:1807.07062 (2018).
 - [26] C. R. Harris, K. J. Millman, S. J. van der Walt, R. Gommers, P. Virtanen, D. Cournapeau, E. Wieser, J. Taylor, S. Berg, N. J. Smith, R. Kern, M. Picus, S. Hoyer, M. H. van Kerkwijk, M. Brett, A. Haldane, J. F. del Río, M. Wiebe, P. Peterson, P. Gérard-Marchant, K. Sheppard, T. Reddy, W. Weckesser, H. Abbasi, C. Gohlke, and T. E. Oliphant, *Array programming with NumPy*, *Nature* **585**, 357 (2020).
 - [27] J. Janquart, O. A. Hannuksela, K. Haris, and C. Van Den Broeck, A fast and precise methodology to search for and analyse strongly lensed gravitational-wave events, *MNRAS* **506**, 5430 (2021).
 - [28] R. K. Lo and I. Magaña Hernandez, Bayesian statistical framework for identifying strongly lensed gravitational-wave signals, *PRD* **107**, 123015 (2023).
 - [29] D. H. Cheung, S. Rinaldi, M. Toscani, and O. A. Hannuksela, Mitigating the effect of population model uncertainty on strong lensing bayes factor using nonparametric methods, arXiv preprint arXiv:2308.12182 (2023).
 - [30] J. Janquart, K. Haris, O. A. Hannuksela, and C. Van Den Broeck, The return of golum: improving distributed joint parameter estimation for strongly lensed gravitational waves, *MNRAS* **526**, 3088 (2023).
 - [31] A. Barsode, S. Goyal, and P. Ajith, Fast and efficient bayesian method to search for strongly lensed gravitational waves, *ApJ* **980**, 258 (2025).
 - [32] O. A. Hannuksela, K. Haris, J. Janquart, H. Narola, H. Phurailatpam, J. D. Creighton, and C. V. den Broeck, Strong gravitational-wave lensing posterior odds (2025).
 - [33] R. K. Lo, denmarf: a python package for density estimation using masked autoregressive flow, arXiv preprint arXiv:2305.14379 (2023).
 - [34] M. Wright, J. Janquart, P. Cremonese, J. C. L. Chan, A. K. Y. Li, O. A. Hannuksela, R. K. L. Lo, J. M. Ezquiaga, D. Williams, M. Williams, G. Ashton, R. Udall, A. More, L. Uronen, A. Barsode, E. Seo, D. Keitel, S. Goyal, J. Heynen, A. Liu, and P. Pankunni, Lensingflow: an automated workflow for gravitational wave lensing analyses, *RASTI* **5**, rzag003 (2026), <https://academic.oup.com/rasti/article->

- pdf/doi/10.1093/rasti/rzag003/66395542/rzag003.pdf.
- [35] LIGO-Virgo-KAGRA Collaboration, Gravitational-wave candidate event database (gracedb) (2024).
- [36] A. Abac, I. Abouelfettouh, F. Acernese, K. Ackley, C. Adamcewicz, S. Adhichary, D. Adhikari, N. Adhikari, R. Adhikari, V. Adkins, *et al.*, Gwtc-4.0: Searches for gravitational-wave lensing signatures, arXiv preprint arXiv:2512.16347 (2025).
- [37] Q. Hu, H. Narola, J. Heynen, M. Wright, J. Veitch, J. Janquart, and C. V. D. Broeck, Gw231123: Overlapping gravitational wave signals?, arXiv preprint arXiv:2512.17550 (2025).
- [38] V. De Luca, G. Franciolini, and A. Riotto, Gw231123: A possible primordial black hole origin, arXiv preprint arXiv:2508.09965 (2025).
- [39] C. Yuan, Z.-C. Chen, and L. Liu, Gw231123 mass gap event and the primordial black hole scenario, Physical Review D **112**, L081306 (2025).
- [40] S. Goyal, H. Villarrubia-Rojo, and M. Zumalacargui, Across the universe: Gw231123 as a magnified and diffracted black hole merger, arXiv preprint arXiv:2512.17631 (2025).
- [41] J. C. Chan, J. M. Ezquiaga, R. K. Lo, J. Bowman, L. M. Zertuche, and L. Vujeva, Discovering gravitational waveform distortions from lensing: a deep dive into gw231123, arXiv preprint arXiv:2512.16916 (2025).
- [42] A. Chakraborty and S. Mukherjee, The first model-independent upper bound on micro-lensing signature of the highest mass binary black hole event gw231123, arXiv preprint arXiv:2512.19077 (2025).
- [43] X. Shan, H. Yang, and S. Mao, Gw231123: A case for binary microlensing in a strong lensing field, arXiv preprint arXiv:2512.19118 (2025).
- [44] B. Wang and T. Yang, Gw231123: False massive graviton signatures from unmodeled point-mass lensing, arXiv preprint arXiv:2604.08179 (2026).
- [45] M. Vallisneri, Testing general relativity with gravitational waves: A reality check, Physical Review D—Particles, Fields, Gravitation, and Cosmology **86**, 082001 (2012).
- [46] W. D. Pozzo, K. Grover, I. Mandel, and A. Vecchio, Testing general relativity with compact coalescing binaries: comparing exact and predictive methods to compute the bayes factor, Classical and Quantum Gravity **31**, 205006 (2014).
- [47] S. Bini, K. Król, K. Chatziioannou, and M. Isi, Impact of waveform systematics and gaussian noise on the interpretation of gw231123, Physical Review D **113**, 083036 (2026).
- [48] C. Chatterjee, K. McGowan, S. Deshmukh, N. Tyler-Howard, and K. Jani, Machine learning confirms gw231123 is a “lite” intermediate mass black hole merger, The Astrophysical Journal Letters **995**, L6 (2025).
- [49] A. Ray, S. Banagiri, E. Thrane, and P. D. Lasky, Gw231123: extreme spins or microglitches?, arXiv preprint arXiv:2510.07228 (2025).
- [50] A. Sasli, N. Karnesis, and N. Stergioulas, Heavy-tailed likelihoods for robustness against data outliers: Applications to the analysis of gravitational wave data, Physical Review D **108**, 103005 (2023).
- [51] J. C. Chan, E. Seo, A. K. Li, H. Fong, and J. M. Ezquiaga, Detectability of lensed gravitational waves in matched-filtering searches, PRD **111**, 084019 (2025).
- [52] J. C. Chan, L. M. Zertuche, J. M. Ezquiaga, R. K. Lo, L. Vujeva, and J. Bowman, Identification and characterization of distorted gravitational waves by lensing using deep learning, Physical Review D **113**, 024041 (2026).
- [53] T. Islam, J. Roulet, and T. Venumadhav, Factorized parameter estimation for real-time gravitational wave inference, arXiv preprint arXiv:2210.16278 (2022).
- [54] P. Virtanen, R. Gommers, T. E. Oliphant, M. Haberland, T. Reddy, D. Cournapeau, E. Burovski, P. Peterson, W. Weckesser, J. Bright, S. J. van der Walt, M. Brett, J. Wilson, K. J. Millman, N. Mayorov, A. R. J. Nelson, E. Jones, R. Kern, E. Larson, C. J. Carey, Í. Polat, Y. Feng, E. W. Moore, J. VanderPlas, D. Laxalde, J. Perktold, R. Cimrman, I. Henriksen, E. A. Quintero, C. R. Harris, A. M. Archibald, A. H. Ribeiro, F. Pedregosa, P. van Mulbregt, and SciPy 1.0 Contributors, SciPy 1.0: Fundamental Algorithms for Scientific Computing in Python, Nature Methods **17**, 261 (2020).
- [55] A. Abac, I. Abouelfettouh, F. Acernese, K. Ackley, C. Adamcewicz, S. Adhichary, D. Adhikari, N. Adhikari, R. Adhikari, V. Adkins, *et al.*, Gwtc-4.0: Population properties of merging compact binaries, arXiv preprint arXiv:2508.18083 (2025).
- [56] P. Madau and M. Dickinson, Cosmic star-formation history, Annual Review of Astronomy and Astrophysics **52**, 415 (2014).
- [57] T. E. Collett, The population of galaxy–galaxy strong lenses in forthcoming optical imaging surveys, ApJ **811**, 20 (2015).
- [58] R. Kormann, P. Schneider, and M. Bartelmann, Isothermal elliptical gravitational lens models, Astronomy and Astrophysics (ISSN 0004-6361), vol. 284, no. 1, p. 285–299 **284**, 285 (1994).
- [59] M. Fukugita and E. L. Turner, Gravitational lensing frequencies-galaxy cross-sections and selection effects, MNRAS **253**, 99 (1991).
- [60] LIGO-Virgo Collaboration, Noise curves used for simulations in the update of the observing scenarios paper (2020), LIGO Document T2000012-v1.
- [61] G. Pratten, C. García-Quirós, M. Colleoni, A. Ramos-Buades, H. Estellés, M. Mateu-Lucena, R. Jaume, M. Haney, D. Keitel, J. E. Thompson, *et al.*, Computationally efficient models for the dominant and subdominant harmonic modes of precessing binary black holes, Physical Review D **103**, 104056 (2021).